Investigations on dielectric and structural properties of ferroelectric betaine phosphite (BPI)

1995 J. Phys.: Condens. Matter 7 9305

(http://iopscience.iop.org/0953-8984/7/48/019)

J. Phys.: Condens. Matter 7 (1995) 9305–9319. Printed in the UK

Investigations on dielectric and structural properties of ferroelectric betaine phosphite (BPI)

H Ebert†, S Lanceros-Méndez†, G Schaack† and A Klöpperpieper‡

† Physikalisches Institut der Universität Würzburg, 97074 Würzburg, Germany

‡ Fachbereich Physik der Universität des Saarlandes, 66123 Saarbrücken, Germany

Received 6 March 1995, in final form 14 July 1995

Abstract. We have extended earlier measurements made on the phase diagram of betaine phosphite (BPI) under hydrostatic pressure by observing the anomalies in the real and the imaginary parts of the dielectric function (ϵ' and ϵ'') and the dissipation factor ($\tan\delta$), especially in the ferroelectric (f) phase at various temperatures (23 K $< T <$ 300 K) and hydrostatic pressures ($p <$ 300 MPa) at frequencies ν = 0.5, 1, 5, 10, 50, 100 kHz. Below the transition into the f phase at T_{c2}, $\tan\delta$ displays a double-peak structure with a large dispersion in our frequency range and a large pressure dependence, both peaks merging for low pressures. The anomalous behaviour found in $\tan\delta$ points to the existence of a distribution of relaxation times and competing dynamics in the 'ordered' phase. The relaxational behaviour of the low-temperature peak could indicate a transition into a glasslike phase in this pure compound. In order to clarify the nature of these new regions in the phase diagram we have studied BPI by means of Raman scattering between 20 and 3150 cm^{-1} and by far-infrared reflection between 15 and 600 cm^{-1}.

1. Introduction

Several addition compounds of the amino acid betaine ($(CH_3)_3NCH_2COO^-$) and inorganic acids display interesting structural phase transitions. Ferroelectric (f), antiferroelectric (af), ferroelastic and modulated phases have been found and are currently the subject of investigations [1, 2]. Betaine arsenate (H_3AsO_4, BA, f), betaine phosphate (H_3PO_4, BP, af), and betaine phosphite (H_3PO_3, BPI, f) are structurally very closely related and mixed crystals are formed accordingly: BA_xBP_{1-x}, BP_xBPI_{1-x}, $0 \leqslant x \leqslant 1$. Glassy phases attributed to frustrated ferroelectric and antiferroelectric interactions, and proton glass behaviour were proposed for some mixed crystals of these families (BA_xBP_{1-x} [3, 4, 5] and BP_xBPI_{1-x} [6, 7, 7a]) and also for the pure compound BA [8, 9]. Such cooperative effects with competing interactions and frustration that lead to orientational glasses are indeed a challenging problem, both experimentally and theoretically [10, 11]. In order to shed new light on the mechanisms underlying the phase transitions in betaine compounds in general and their glassy phases in particular we have investigated BPI with a small percentage of impurities or defects (most probably BP, $\approx$1.5%).

Ferroelectric BPI [$(CH_3)_3NCH_2COOH_3PO_3$] is a molecular crystal of betaine and phosphorous acid. Its structure is characterized by the linking via hydrogen bonds of the inorganic PO_3 tetrahedra, in which the missing O, with respect to PO_4^{2-}, is replaced by a proton, to quasi-one-dimensional chains along the monoclinic axis, each betaine being attached via O–H$\cdots$O bonds to these inorganic units (figure 1, lower panel). The

0953-8984/95/489305+15$19.50

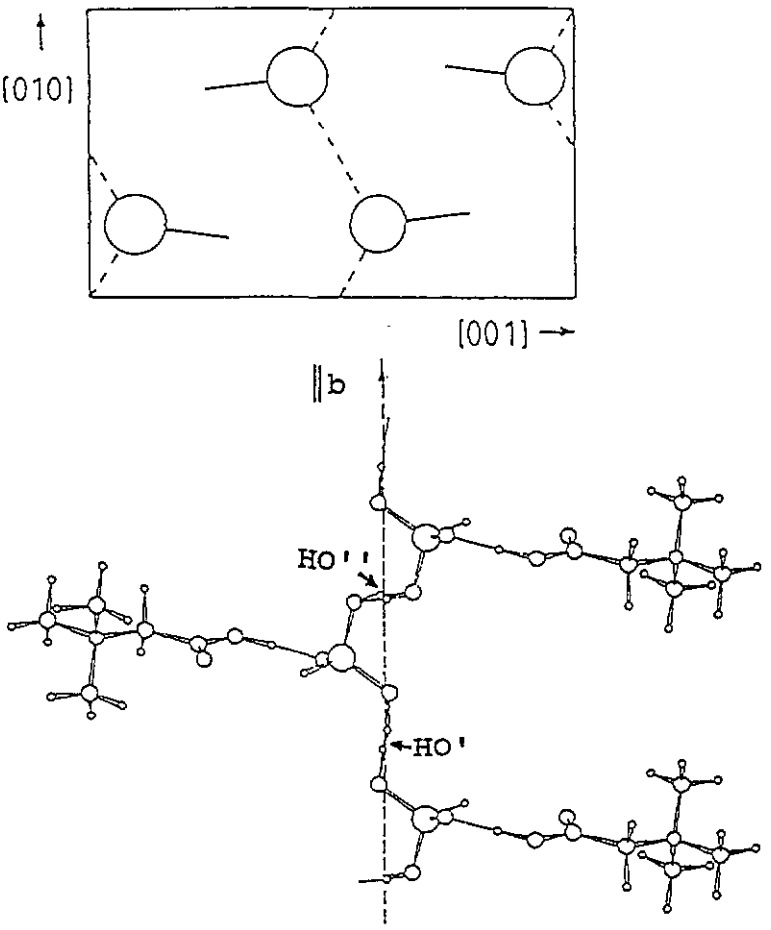

Figure 1. The top panel shows schematically the structure of the unit cell at room temperature [12]. Circles: tetrahedra; full lines: betaine molecules; dashed lines: H bonds. The bottom panel shows the structure of BPI along the y (monoclinic and polarization) axis from [16].

betaine units are oriented almost perpendicularly to the quasi-one-dimensional chains. Ferroelectricity appears along the direction of the hydrogen-bonded chains. This compound shows a sequence of three phase transitions: a structural high-temperature transition at $T_{c1} = 355$ K, one to a f phase with a maximum in ϵ' at T_{c2} (224 K > T_{c2} > 208 K [12, 16]) and a further transition at $T_{c3} = 177$ K not clarified for the moment. BPI is monoclinic at room temperature ($P2_1/c$) with four molecules per unit cell (figure 1, upper panel) [1, 13, 14, 15, 16]; the spontaneous polarization below T_{c2} occurs along 2_1, [010]. The transition temperature T_{c2} appears to be extremely sensitive to a small percentage of impurities (PO_4^{3-}) or to crystalline defects.

It has been shown with ^{1}H-electron–nuclear-double-resonance (ENDOR) techniques [17] that the protons interconnecting the PO_3 tetrahedra (HO′ and HO″ in figure 1, upper panel) are ordered below T_{c2} in one minimum of the symmetrical ($T > T_{c2}$) double-well potential of an O–H···O bond [12], giving rise to long-range order below T_{c2} in the chains. Such configurations of the protons only exist where the HO′ proton is close to a specific tetrahedron and the HO″ proton is far away or vice versa. Thus a polarization of the tetrahedra along the axis is induced by the protons. The phase transition at T_{c2} is thus

of the order–disorder type. The symmetrical H-bond potential is distorted asymmetrically for $T \leqslant T_{c2}$. The observed shift of T_{c2} on deuteration (216 K $\rightarrow$ 297 K [12]) and the destabilization of the ordered phase on applying hydrostatic pressure [12] due to the lowering of the central barrier in the double-well potential are in accordance with this interpretation. Below T_{c2} the PO_3^{2-} groups within the chains are tilted and slightly distorted with respect to the antiferrodistortive room-temperature phase according to the disappearance of the mirror glide-plane ($P2_1/c \rightarrow P2_1$, point group $C_{2h} \rightarrow C_2$) at T_{c2}. The ferroelectric phase of BPI is a very fragile structure: small admixtures of BP and the occurrence of crystalline defects [12] lower T_{c2} drastically. This becomes evident from the BP_xBPI_{1-x} phase diagram [18]: for $x = 0.1$ the transition temperature T_{c2} drops to $\approx$36 K. In a mixed crystal, $BP_{0.15}BPI_{0.85}$, a dielectric anomaly indicating a transition into a ferroelectric phase is not found; however, the occurrence of a glassy phase ($T_g = 40$ K) is encountered [19]. Our crystal with a small percentage of impurities is an interesting example as regards the observation of precursor effects of this glassy phase. We expect deviations from the strict rule of the proton configuration in the H bonds mentioned above, and interconnecting and polarizing the PO_3^{2-} tetrahedra. It has in fact been observed in $BP_{0.15}BPI_{0.85}$ that beside the 'regular' configuration (HO′ close and HO″ far, or HO′ far and HO″ close), the 'irregular' configurations (HO′ close and HO″ close, and HO′ far and HO″ far) occur with equal probability. The PO_3^{2-} tetrahedra are tilted and distorted differently; no long-range order is observed but an Edwards–Anderson glass order parameter can be determined. It is to be expected that in our sample with low BP doping, irregularities in the proton configuration at or near the BP centres will occur and show up both in dielectric and spectroscopic experiments. Even in nominally pure BPI ($T_{c2} = 224$ K) [20] a deviation from a monodispersive (Debye-type) relaxation behaviour is observed close to T_{c2} and is related to crystal lattice defects.

2. Experimental details

The crystal was grown by controlled evaporation from aqueous solution and oriented using polarized light and x-ray Laue backscattering along the monoclinic axis. For the dielectric measurements, samples in the shape of thin slices ($\approx 5 \times 5 \times 0.9$ mm^3) were cut perpendicular to the monoclinic axis and polished. Vacuum-deposited aluminium films served as electrodes. The dependences on temperature (23–300 K), hydrostatic pressure (<300 MPa), and frequency (0.1–100 kHz) of ϵ' and $\tan\delta$ ($=D = \epsilon''/\epsilon'$) were measured with a standard *LCZ*-meter (Keithley, model 3322). The field strength was always approximately 11 V cm^{-1} at zero d.c. field. Helium gas was used as the pressure-transmitting medium. For the Raman experiments, oriented samples in the shape of cubes (approximately $8 \times 5 \times 5$ mm^3) were optically polished; the spectra were excited with the linearly polarized 514.5 nm line of an argon-ion laser with a power of about 130 mW. The light was scattered through 90° and analysed with a Dilor XY spectrometer for the accessible symmetries in each phase in the phase diagram, between 15 and 3150 cm^{-1}. For the far-infrared reflection spectroscopy the samples in the shape of thin slices (approximately $6.5 \times 6.5 \times 1.6$ mm^3) were cut parallel to the monoclinic axis and optically polished. Two spectra in each different phase were taken for the accessible symmetries between 15 and 600 cm^{-1}.

2.1. Dielectric measurements

2.1.1. Experimental results. In figure 2 ϵ' and $\tan\delta$ are shown for $p = 75$ (top) and 350 MPa (bottom) and for several frequencies. Figure 3 presents the pressure dependence

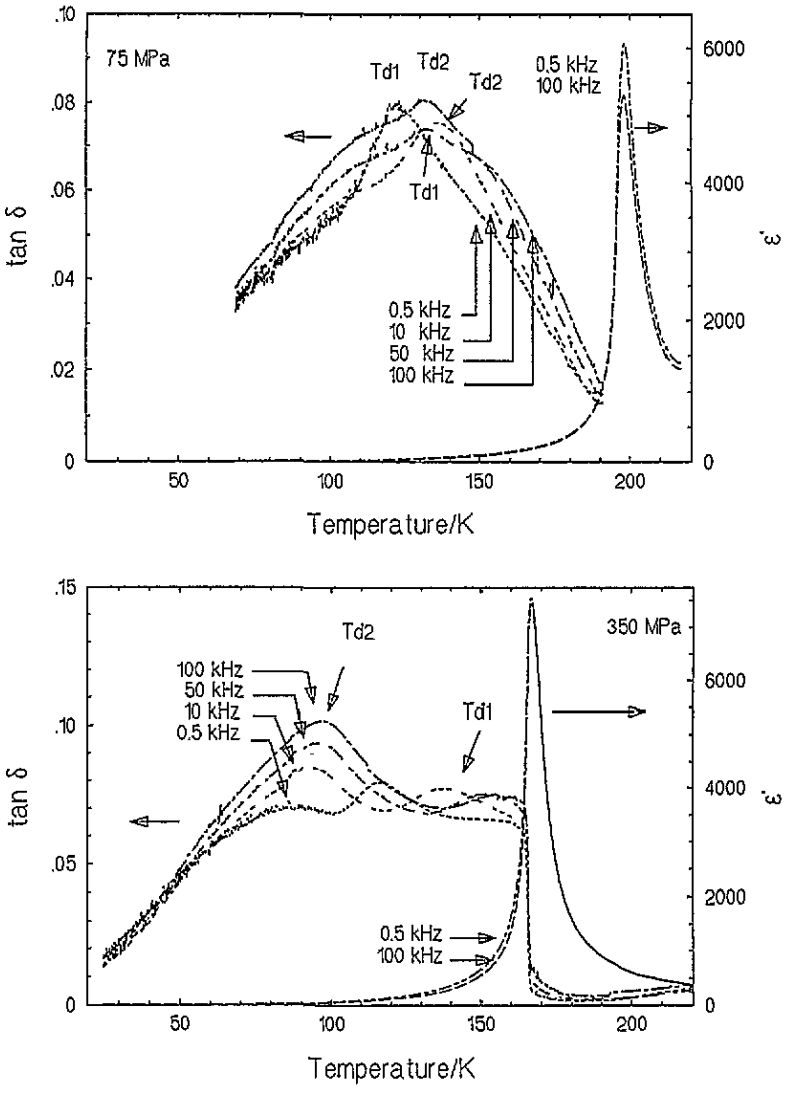

Figure 2. Temperature dependences of ε' and $\tan\delta$ for BPI at 75 MPa (above) and 350 MPa (below) at various frequencies.

of the dissipation factor for 100 kHz (top) and 500 Hz (bottom). The maximum in ϵ' at T_{c2} shifts to lower temperatures with increasing pressures; the ordered phase is destabilized. We obtain

$$T_{c2}(p) = (206 \pm 2.5)\ \mathrm{K} - p \times 0.112\ \mathrm{K\ MPa^{-1}} \tag{1}$$

where the slope agrees well with earlier results [12]. We have found a lower value of T_{c2} ($p = 0$) than other groups (224 K [20], 216 K [7a], 208 K [12]). We attribute this variation in the transition temperature for different samples to minute amounts of impurities, especially PO_4 ions. We observe no changes in the shape of the ϵ'-anomalies with pressure. At $T < T_{c2}$ a small dispersion is observed in ϵ' at high p; at $T \approx T_{c2}$ a frequency dependence in the value of the maximum is found. The first effect decreases while the second increases

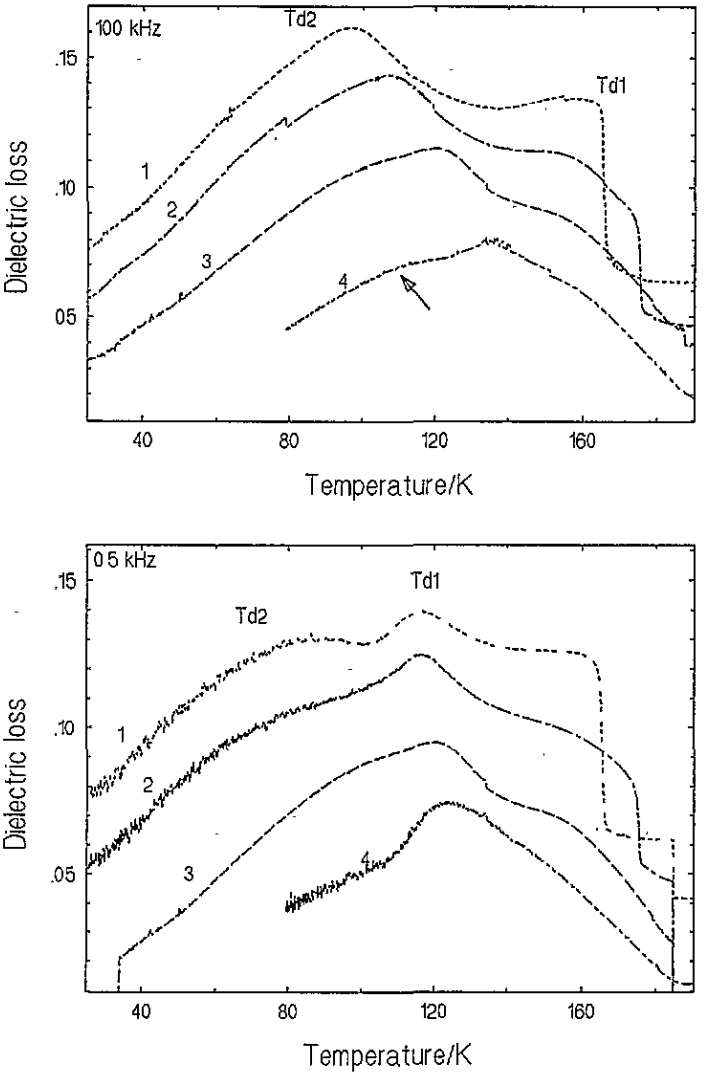

Figure 3. The pressure dependences of the dissipation factor $\tan\delta$ at 100 kHz (above) and 500 Hz (below). 1: 340; 2: 260; 3: 165; 4: 50 MPa. Offset: 0.02.

with decreasing pressure (figure 2). We measure a small thermal hysteresis of about 4 K. Due to the error in our experimental data of ± 0.5 K it is difficult to estimate the true size of this effect; nevertheless comparison with the thermal hysteresis of the other peaks in the phase diagram confirms that the hysteresis exists and is not an effect of the measurement devices (figure 4). A transition type close to second order but with a first-order tendency as proposed by Narz [15] is thus confirmed, and it is in agreement with the conclusions of Launer *et al* [12]. In our measurements the most conspicuous feature is the behaviour of $\tan\delta$ (figures 2 and 3), i.e. its two-peak structure and the frequency and pressure dependence of both peaks. Some experimental facts are worth mentioning.

(i) At high pressure $\tan\delta$ develops a double-peak structure (figure 2, lower panel). The high-temperature peak, with a maximum at T_{d1}, shows a large frequency variation in the

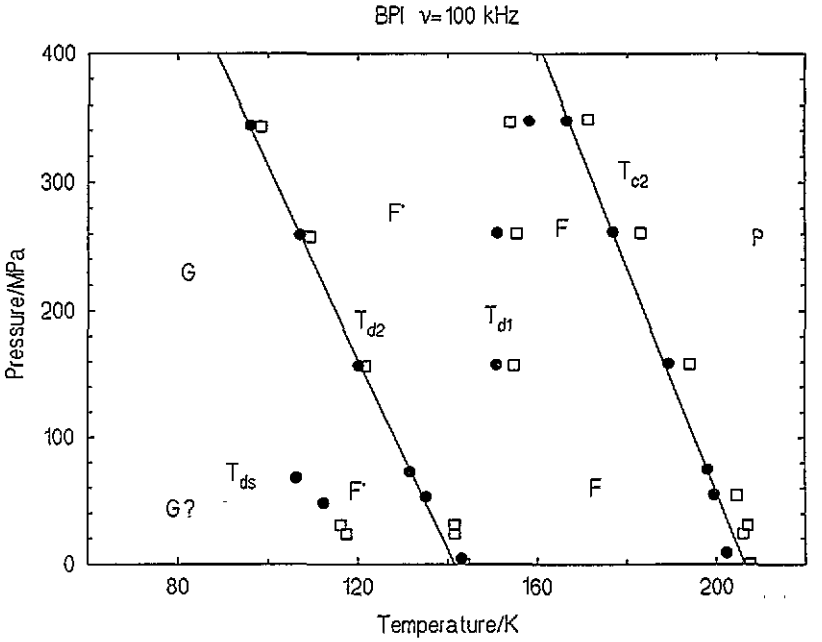

Figure 4. The (p, T) phase diagram of BPI at 100 kHz. P: paraelectric; F: ferroelectric; F': pseudoferroelectric; G: frozen phases. The circles correspond to $dT/dt < 0$ and the squares to $dT/dt > 0$.

position of its maximum but presents a rather stable size. On the other hand, the low-temperature peak (T_{d2}) is strongly dependent on frequency, but the peak position changes only slightly with frequency.

(ii) The maxima in $\tan\delta$ shift to lower temperatures as the frequency is decreased (figure 2).

(iii) The shape of the $\tan\delta$ anomaly also changes under pressure. With lowering pressures T_{d2} shifts to higher temperatures, while T_{d1} appears to show only a small shift to lower temperatures. For T_{d2} we obtain

$$T_{d2} = (141.5 \pm 3.2)\ \mathrm{K} - p \times 0.132\ \mathrm{K\ MPa^{-1}}. \tag{2}$$

The pressure dependence of T_{d2} differs by only about 14% from the pressure dependence of T_{c2}, which indicates that the two processes might be correlated.

The combined effects of pressure and frequency give, as a result, the definition of three different regions in the ferroelectric phase below T_{c2} (figure 4).

(a) At high pressures peaks T_{d1} and T_{d2} are both observable. With decreasing pressure T_{d2} shifts to higher temperatures and dominates over T_{d1}, which becomes a small shoulder of T_{d2} (figure 3, upper panel).

(b) At low frequencies the height of T_{d2} is smaller than that of T_{d1}, so T_{d1} becomes dominant due to its shift with decreasing pressure (figure 3, lower panel).

(c) At high frequencies and with decreasing pressure a third peak in the dissipation factor at T_{d2} seems to appear (the arrow in figure 3, upper panel).

Figure 4 depicts the (p, T) diagram, where the positions of the maxima of the observed anomalies have been plotted.

2.1.2. Discussion. The imaginary part of the complex dielectric constant is a quantity resulting from response-time delays. The study of ϵ'' or $\tan\delta$ appears to be especially appealing in the investigation of glassy systems [21]. Glasslike systems and relaxor ferroelectrics are characterized by a broad distribution of relaxation times, large frequency dependence of anomalies and high dielectric losses below the freezing transition. Such effects are derived from our present experimental data on the weakly doped compound BPI. From the study of the experimental facts some interesting conclusions about BPI and other betaine compounds can be drawn. First of all, the growth of $\tan\delta$ after the transition into the f phase with the two loss peaks together with their different frequency and pressure dependencies is evidence of the existence of two different dynamic processes within the f phase. These processes, which are coupled at normal pressure, are continuously uncoupled under hydrostatic pressure giving rise to two freezing scenarios. The anomaly at T_{d1} indicates the onset of a freezing process. Whether this process is due to the freezing of some molecular groups independently of the dipole degrees of freedom or to the dipole structure cannot be established at the moment. The low-temperature anomaly in $\tan\delta$ (T_{d2}) should indicate the transition into an eventually disordered region where the freezing of the domain structure occurs. The fact that $\mathrm{d}T_{c2}/\mathrm{d}p \approx \mathrm{d}T_{d2}/\mathrm{d}p$ suggests a correlation between the peak indicating the onset of long-range order and the maximum in $\tan\delta$ indicating the freezing. The similar experimental facts observed for the BA_xBP_{1-x} system [5] and in BCCD [22] at low temperatures indicate that whereas specific interactions are responsible for the different phase behaviours at higher temperatures (in BPI the coupled dynamics of the PO_3 group and the H bonds), the low-temperature behaviours in the betaine compounds are due to a common mechanism responsible for the definite freezing or frustration of the system. As topological disorder is not needed to obtain glassy behaviour, but suitable competition leading to frustration is needed, this mechanism could be attributed to the betaine molecule, a zwitterion with a permanent dipole moment, and its interaction with the dipoles formed in the higher-temperature phases.

In conclusion we distinguish three different regions in the phase diagram of BPI (see figure 4):

(a) the ferroelectric region below T_{c2};

(b) the region between T_{d1} and T_{d2} in which the ferroelectric order is continuously broken due to a freezing process—i.e. a pseudoferroelectric phase (a ferroelectric phase with frozen or frustrated regions); and

(c) a clusterlike phase, with fixed domain structure, below T_{d2} where the definitive freezing of the dipoles occurs.

The pure ferroelectric phase is suppressed by pressure for $p > 350$ MPa. The depicted behaviour can be observed only for $p > 150$ MPa; for $p < 150$ MPa both anomalies in $\tan\delta$ merge and a frequency-dependent 'phase' behaviour is observed. At low frequencies the glass phase is suppressed due to the dominant effect of the T_{d1}-dynamics.

2.2. Spectroscopic measurements

With the phase diagram obtained from the dielectric measurements as a reference, the spectroscopic investigations should show whether or not the observed transitions are identifiable in the spectra, shedding new light on the structural properties of the regions in the phase diagram and the dynamical contribution of the different units of the BPI molecule to the phase transitions.

BPI has $Z = 4$ formula units per unit cell, each consisting of 26 atoms. The results of a

Table 1. Results of the factor group analysis, after [19].

C_{2h}	E	C_2	i	σ_h	*n* (tot)	*n* (aco)	*n* (tra)	*n* (lib)	*n* (vib)
A_g	1	1	1	1	75	0	6	6	63
B_g	1	−1	1	−1	75	0	6	6	63
A_u	1	1	−1	−1	81	1	5	6	69
B_u	1	−1	−1	1	81	2	4	6	69
				$\sum$	312 total	3 acoustic	21 external	24 external	264 internal

factor group analysis corresponding to the relevant point group C_{2h} can be found in [23], and are summarized in table 1. The modes belonging to the representations A_g and B_g are Raman active and they were observed in the $x(yy)z$ and the $x(yx)z$ configuration respectively. The infrared-active modes A_u are polarized along the twofold axis and observed with $\boldsymbol{E} \parallel y$; the B_u modes are observed with $\boldsymbol{E} \perp y$. Although the separation of the modes into external modes, where the molecular groups move as rigid units, and into internal modes at higher frequencies is not totally exact due to the mixing with internal vibrations of the betaine molecule and coupling between the vibrations of different molecular units in the low-frequency region, it is useful for the interpretation of the data. According to this picture we expect 12 translational and 12 librational Raman-active modes and 9 translational and 12 librational infrared-active modes among the total 312 modes. Below T_{c2} the mirror glide-plane, i.e. the centre of inversion, is lost ($C_{2h} \rightarrow C_2$), which raises the spectroscopic parity selection rules valid in C_{2h}. However, the modes additionally allowed below T_{c2} in Raman or infrared spectra are too weak to be observed, i.e. the structural changes at T_{c2} are minute.

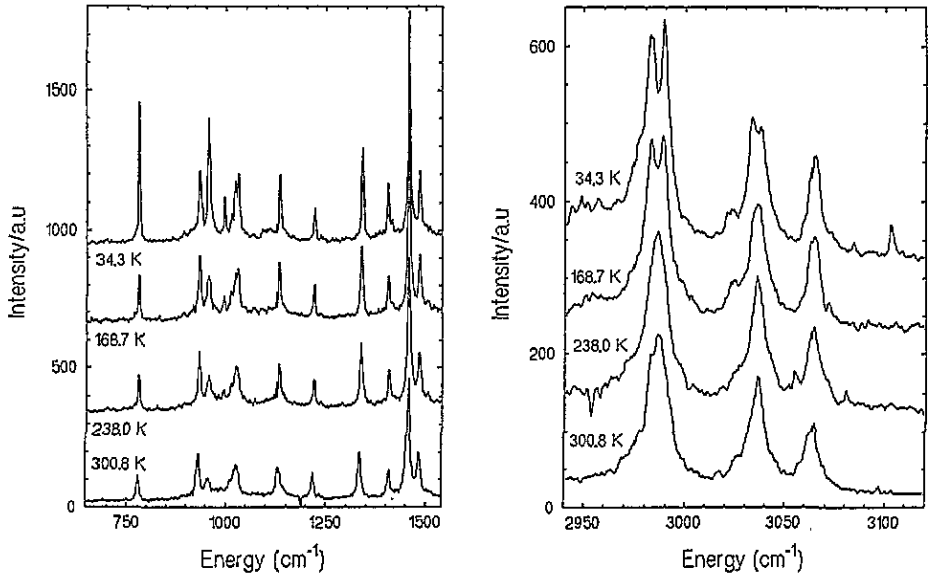

Figure 5. Raman spectra of BPI in B_g symmetry for high frequencies. Only those regions in which mode structures are observed are shown.

2.2.1. Raman measurements between 600 and 3150 cm^{-1}. The spectra were taken between 34 and 300 K in A_g and B_g symmetry (figures 5, 6). With the help of previous investigations [24, 25, 26] we have tried to identify the present internal modes with specific crystal vibrations. One has to take into account that the reference data are for a pure betaine molecule, while in our case the molecule forms part of a BPI crystal. The phosphite tetrahedron, with the point group C_{3v}, has six different degenerate normal modes which we call pure phosphite vibrations [27]. These tetrahedron vibrations must be seen, due to the raising of the degeneracy in all the symmetries, as a group of various lines. The results are as follows.

(i) At 780 cm^{-1}†, in both symmetries, a sharp mode exists that can be identified with a betaine vibration [25].

(ii) Between 900 and 1050 cm^{-1} is a group of three sharp (A_g), and five to six broad (B_g) modes present in both symmetries. These peaks can be identified with a C–H deformation vibration in the betaine molecule [25]. On the other hand, in this region a symmetric PO_3 stretching vibration and a twofold-degenerate asymmetric P–H deformation are present according to Tsuboi [26]. Wide groups of modes between 2900 and 3100 cm^{-1} representing C–H valence vibrations were also found in both symmetries.

(iii) In A_g symmetry the asymmetric PO_3-stretching vibration was identified as a weak line at 1100 cm^{-1} [26], at low temperatures, and a P–H stretching vibration was identified as a sharp mode at 2380 cm^{-1}.

(iv) In the spectral range between 1100 and 1500 cm^{-1}, sharp modes are present especially in B_g symmetry, identified as C–H deformation vibrations and C–O vibrations.

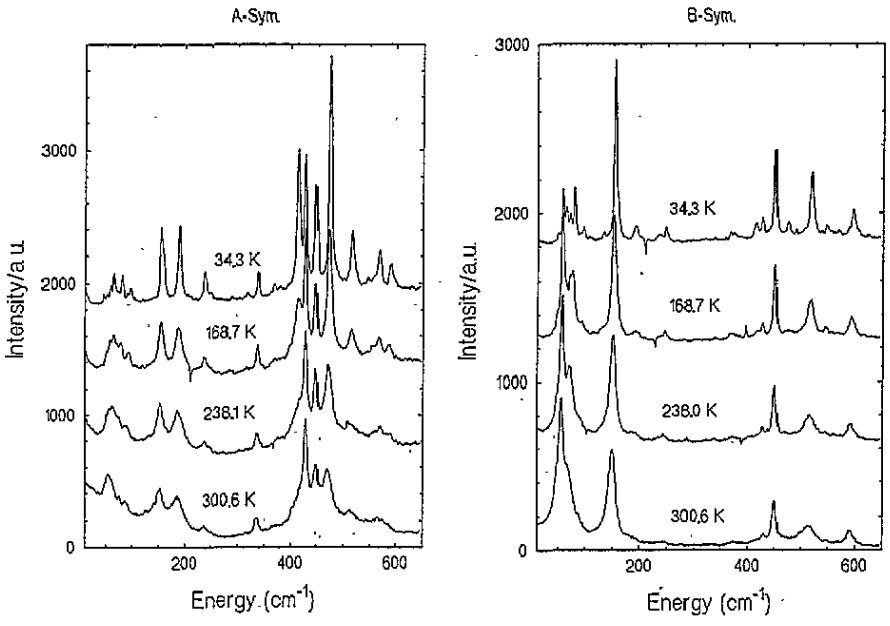

Figure 6. Raman spectra of BPI in A_g and B_g symmetries for low frequencies.

2.2.2. Raman measurements between 15 and 600 cm^{-1}. With respect to phase transitions, the spectroscopic investigation of the low-energy region plays an important role. The

† The energy values are taken from the lowest-temperature spectrum.

results of the Raman measurements are presented for the two symmetries in figure 6. For the interpretation of these data we tried at first the identification of specific phosphite and betaine vibrations; secondly, we looked for phase-specific changes in the mode structure, new modes and soft modes. The solution of these problems will finally shed new light on the mechanisms of the phase transitions in this compound and eventually on the atomic vibrations responsible for the changes.

(A) Internal vibrations. For the identification of pure betaine vibrations we have made use of the data of Schrader [25]. We could identify:

(i) betaine vibrations in A_g symmetry at 237, 339, 428, 448, 545 cm^{-1};
(ii) betaine vibrations in B_g symmetry at 153, 427, 450, 595 cm^{-1}.

In all these modes, except a slight energy displacement, a dependence on temperature or phase could not be found.

For the free phosphite tetrahedron only two modes at ν_1 ($\sim$E) = 459 cm^{-1} and ν_2 ($\sim$A) = 550 cm^{-1} should be observable in this spectral range [26]. These modes could not be definitely identified, possibly because the eigenfrequencies of the PO_3 tetrahedra are shifted with respect to these energies by the crystalline environment and the superposition on and mixing with betaine vibrations.

In any case, by comparison of the Raman spectra with known IR spectra [23], it was possible to identify some of the internal vibrations of the tetrahedra.

(i) In A_g symmetry a new mode appears at 414 cm^{-1} at the transition into the f phase. At the same position an IR-active phosphite vibration was identified [23], which becomes Raman active in the f phase.

(ii) Koch *et al* [23] found a phosphite mode at 449 cm^{-1} in A_g symmetry and at 446 cm^{-1} in B_g symmetry. We have observed lines in the same range but, due to being in the neighbourhood of a betaine vibration, a clear identification was not possible.

(B) Phase-dependent changes in the mode structure. With regard to modes which change at the different phase transitions some points are worth mentioning.

(i) In A_g symmetry the most significant changes in the whole spectral range are due to the mode at 414 cm^{-1} appearing in the f phase and increasing in intensity with decreasing temperatures and the continuous splitting of the lowest-energy mode group around 70 cm^{-1} (figure 6).

(ii) In B_g symmetry between 50 and 100 cm^{-1} and at low temperatures a mode loses intensity and splits into a group of seven modes of lower intensity (figure 6).

(iii) This new behaviour at low temperatures is corroborated by another change in the mode structure at 474 cm^{-1} in B_g symmetry too.

2.2.3. Discussion. We have explored the Raman spectroscopic results with particular attention paid to aspects relevant to the freezing process suggested in the dielectric measurements—especially whether or not the transformation affects betaine or tetrahedra modes, and leakage of bands into scattering symmetries where they are not allowed on the basis of the high-temperature crystal structure, as well as internal vibration frequencies.

First we have identified modifications in the internal vibrations of the betaine molecule up to the lowest temperatures and especially after the transition at T_{d2}—for example, the group of modes around 1000 cm^{-1} in figure 5, which point to the activity of this molecule in the low-temperature phase. The temperature dependence of the mode appearing at 414 cm^{-1} in A_g symmetry, identified as a phosphite vibration, and some betaine modes (for example

that at 474 cm^{-1} in A_g symmetry), which pick up intensity progressively upon cooling to the low-temperature region, is a strong indication that the formation of the new 'phase' is to be associated with the fixing of this vibration, as that fixing is necessary to obtain a well-defined line.

As the frozen or glass-type phase forms, the symmetry breaking should become more severe causing both leakage into other symmetry types and splitting of degenerate modes. This seems to be indicated for some weak modes in the lowest-temperature spectra (figure 6) and for the group of modes in the lowest-energy region (figure 6): upon cooling and especially in B_g symmetry the mode loses intensity and at low temperature splits into a group of seven modes of lower intensity. These effects point to different relative orientations of the betaine molecule or, more probably, different orientations or surroundings (H bonds) of the phosphite tetrahedron as responsible for the low-temperature behaviour. The lowest modes near 45 cm^{-1} in the A_u and B_u spectra were attributed to external librational or translational motions of the PO_3 tetrahedron [23]. Taking into account the permanent dipole of the betaine molecule and that of the PO_3 coupled with the H-bond fixing this seems a possible mechanism for explaining the dielectric behaviour.

In any case the Raman spectra changes indicate that at low temperatures structural changes occur, and reinforce the data from the dielectric measurements.

2.2.4. IR reflection measurements. We have also investigated BPI by means of IR reflection measurements between 17 and 290 K in the range 15–600 cm^{-1} (figure 7). As for the Raman spectra, first of all we tried to identify pure betaine and phosphite vibrations by comparison with the existing measurements for the pure compounds. After this we fitted the modes with independent damped Lorentzian oscillators:

$$\epsilon(\omega) = \epsilon_\infty + \sum_i \frac{\Delta\epsilon_i \nu_i^2}{\nu_i^2 - \nu^2 + i\nu\gamma_i}. \tag{3}$$

This enables us to investigate quantitatively the modes with respect to their energy (ν_i), damping (γ_i) and dielectric strength ($\Delta\epsilon_i$), observing especially those modes with anomalies in these parameters at the different phase transitions.

(A) Internal vibrations. With help of the data of Schrader [25] we have identified some pure betaine vibrations:

(i) in A_u symmetry we could identify a mode group between 150 and 200 cm^{-1} and a clear line at 445 cm^{-1};

(ii) in B_u symmetry a light line appears at 240 cm^{-1} and another vibration at 595 cm^{-1}.

For the identification of pure phosphite vibrations the situation is the same as for the Raman measurements. On using the same approximations, vibrations of the tetrahedra can be supposed to occur in the regions described as follows [23]:

(i) in A_u symmetry a mode at 414 cm^{-1} and another one at 445 cm^{-1};

(ii) in B_u symmetry a group of modes around 570 cm^{-1} could be identified as phosphite vibrations.

(B) Phase-specific modes. We have called those modes that show an anomalous behaviour with respect to the three fitting parameters ($\nu_i, \gamma_i, \Delta\epsilon_i$) phase-specific modes. In A_u symmetry, 23 modes were fitted with temperature-dependent frequencies as shown in figure 8. In B_u symmetry, fewer modes are present and the spectra were fitted with 18 oscillators (figure 9). Some of these modes show anomalous behaviour with respect to the damping

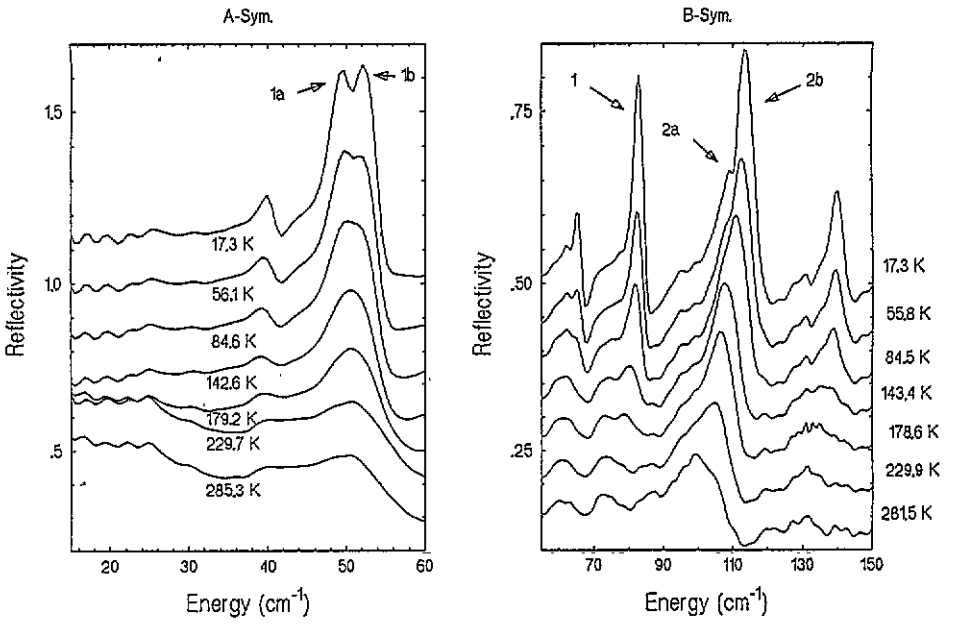

Figure 7. IR reflection spectra of BPI in A_u and B_u symmetries for the low and the intermediate frequency range respectively. The numbered arrows refer to figures 8 to 10.

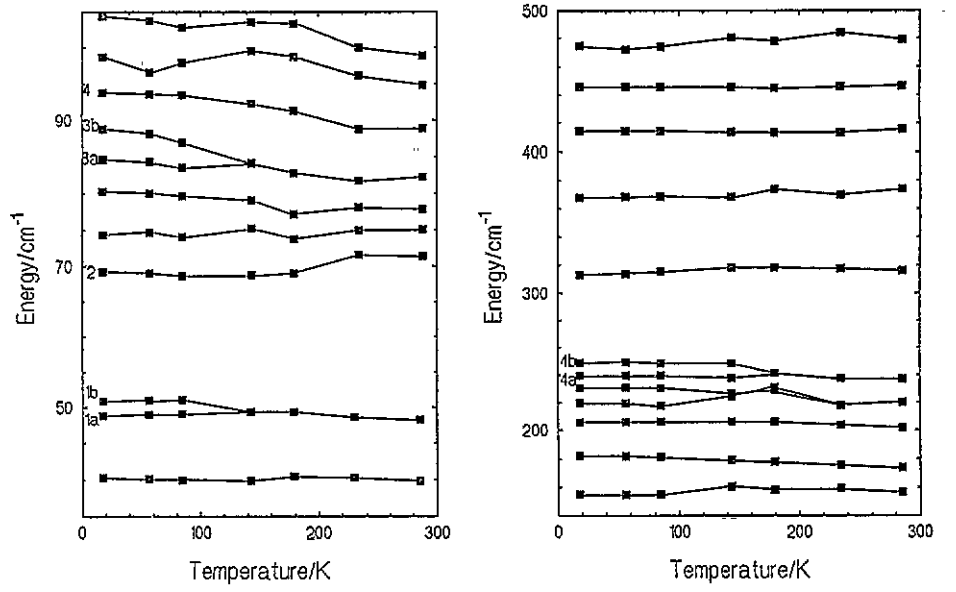

Figure 8. Temperature dependences of the frequencies of the fitted modes in A_u symmetry.

and/or the dielectric strength. These modes are numbered in figures 7, 8, and 9 from low to high wave numbers.

(C) Discussion. Infrared reflection measurements on BPI around the f phase transition at T_{c2} (203 K–323 K) were made for Koch and Happ [23] between 5 and 4000 cm^{-1}. They observed, in the spectra polarized along the f direction, a soft monodispersive relaxation

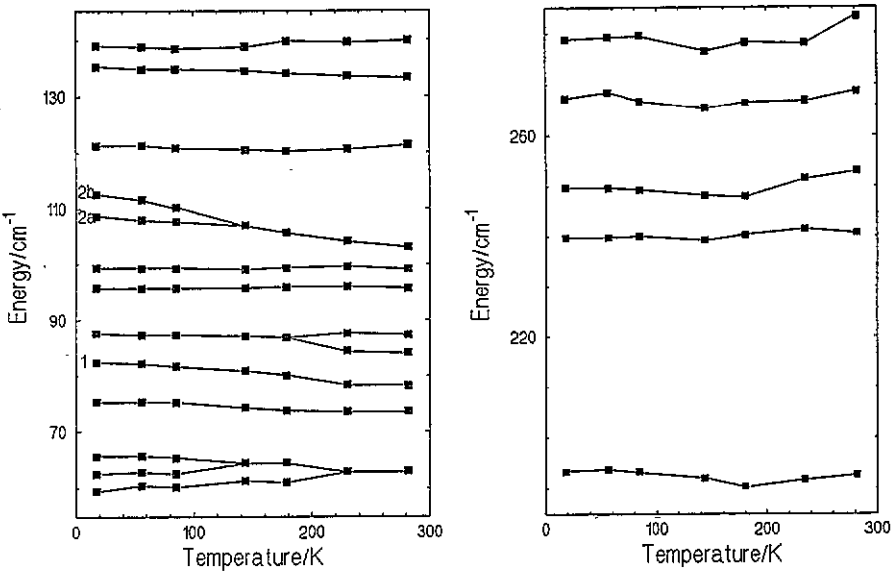

Figure 9. Temperature dependences of the frequencies of the fitted modes in B_u symmetry.

mode below 40 cm^{-1} which accounts for a large part of the relevant static dielectric constant. A similar situation occurs in the f betaine arsenate [28]. In both cases it is concluded that another soft mode must exist in the microwave region. Except that mode and another one at about 58 cm^{-1} in B_u symmetry which exhibits a strong anomalous decrease of damping with increasing temperature, the other oscillator modes exhibit normal temperature dependence.

We have extended the measurements of Koch and Happ down to lower temperatures (~17 K) and we have concentrated our attention on the temperature regions where the anomalies in $\tan\delta$ were found in the dielectric measurements. At the transition at T_{c2} we have not observed the soft relaxational mode. Whether this is due to the lack of accuracy of our experimental set-up in the region below 35 cm^{-1} or due to the impurities and the mixed-crystal character of our sample cannot be established for the moment. The infrared reflection spectra show regions with rich structures and regions in which only noise was observed. Although the modes in the intermediate-wave-number region show an energy displacement at the f phase transition, the energies of the rest of the modes do not show important changes at the transition temperatures. Some modes (especially mode 2 in B_u and modes 3 and 4 in A_u symmetry) shift continuously to higher wave numbers with decreasing temperatures. Excluding mode 2 (figure 10) in A_u symmetry, all the modes show a more or less normal damping behaviour. On the other hand, the dielectric strengths of those modes with wave number <100 cm^{-1} present phase-specific behaviour (figure 10).

Basically, the dielectric strength exhibits a strong decrease below either T_{c2} or T_{d2} which is often associated with a splitting or the appearance of new modes (figures 7 and 10). Above these temperatures $\Delta\epsilon_i$ grows slightly with decreasing temperature or remains stable. This shows that some modes are influenced by the transition at T_{c2} while others change with the transition at T_{d2}. Only mode 2 (figure 10) in A_u symmetry shows anomalies at the two transition temperatures: one at T_{d1} in the damping and two anomalies at T_{c2} and T_{d2} in the dielectric strength. A third special feature is the growth of $\Delta\epsilon_i$ at $T = 17$ K, which in this case could be an error in the fit. It is interesting that some modes become extremely narrow below the transition at T_{d2}—modes 1 and 2b in figure 7—which could

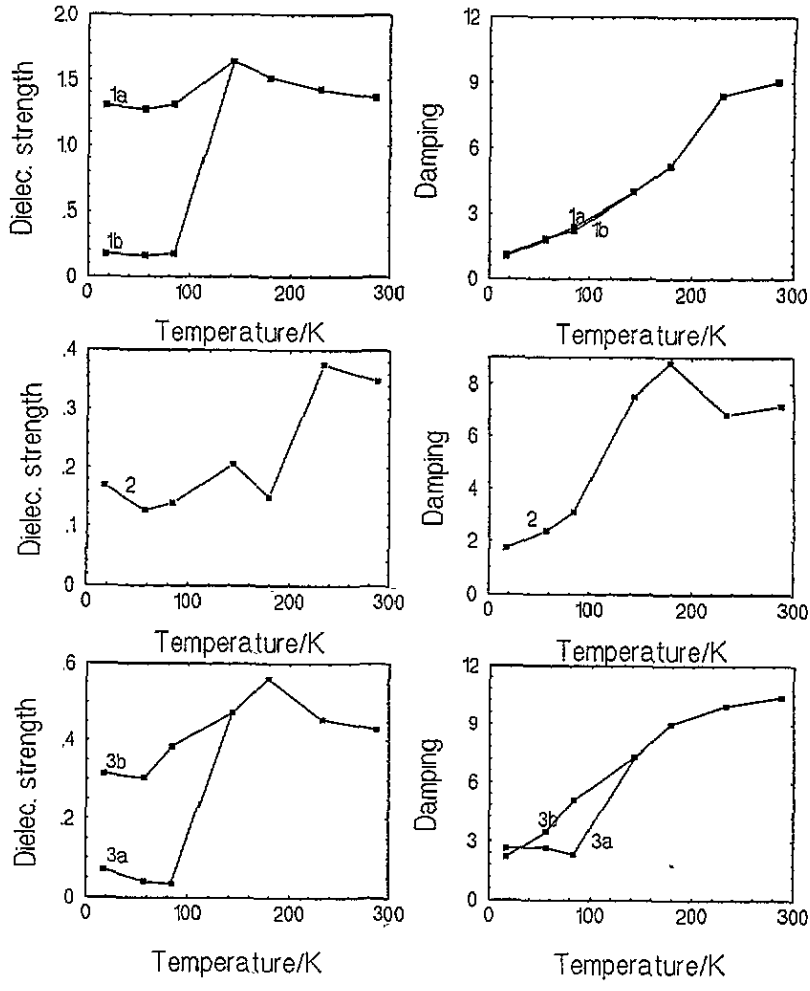

Figure 10. The behaviour with $\Delta\epsilon$ and γ of modes 1a, b, 2 and 3a, b in A_u symmetry.

indicate a lowering of the local symmetry. The results are consistent with the new features found in the dielectric measurements and Raman measurements.

3. Conclusion

We have extended the investigations made on BPI and we have identified two different dynamic processes and structural changes at low temperature within the f phase. The two mechanisms are uncoupled under hydrostatic pressure giving rise to two different freezing scenarios. The sequence of the anomalies depends on the measurement frequency at low pressures. The interpretation of these data can shed new light on the mechanisms of the different phase transitions in betaine compounds, pointing to the participation of the betaine molecule in the low-temperature behaviour. The observed low-temperature anomalies are due to a relaxation process and thus there is no sharp transition into the new low-temperature region in the phase diagram. The freezing is associated not with a static phenomenon but with a relaxational one. The experimental fact of the frequency dependence of some of the

low-temperature 'phases' indicates the existence of slowly relaxing metastable states. Of course, some additional experimental work is necessary in order to clarify whether these phenomena occur in the pure compound or are due to the impurities, the nature of the low-temperature behaviour, the mechanisms responsible for that behaviour, and the relation to that found in other betaine compounds.

Acknowledgments

We thank M Rösch and M le Maire for useful comments on the manuscript and J Kraus for technical support. The support from the Basque Government under grant BFI94.092 is gratefully acknowledged by SLM.

References

[1] Albers J 1988 *Ferroelectrics* **78** 3
[2] Schaack G 1990 *Ferroelectrics* **104** 147
[3] Maeda M 1989 *Ferroelectrics* **96** 269
Maeda M and Suzuki I 1990 *Ferroelectrics* **108** 351
[4] Hayase S, Koshiba T, Terauchi H, Maeda M and Suzuki I 1989 *Ferroelectrics* **96** 221
[5] Lanceros-Méndez S, le Maire M, Schaack G, Schmitt-Lewen M and Wilhelm C 1994 *Ferroelectrics* **157** 269
Lanceros-Méndez S, Schaack G and Klöpperpieper A 1995 *Ferroelectrics* at press
[6] Santos M L, Azevedo J C, Almeida A, Chaves M R, Pires A R, Müser H E and Klöpperpieper A 1990 *Ferroelectrics* **108** 363
[7] Hutton S L, Fehst I, Böhmer R, Braune M, Mertz B, Lunkenheimer P and Loidl A 1991 *Phys. Rev. Lett.* **66** 1990
[7a] Hutton S L, Fehst I, Böhmer R and Loidl A 1992 *Ferroelectrics* **127** 279
[8] Almeida A, Carbalho P S, Chaves M R and Azevedo J C 1988 *Ferroelectron. Lett.* **9** 107
Almeida A, Carbalho P S, Chaves M R and Pires A R 1990 *Ferroelectrics* **108** 347
[9] Chaves M R and Almeida A 1991 *Phys. Scr.* **T 35** 179
[10] Binder K and Young A P 1986 *Rev. Mod. Phys.* **58** 801
Binder K and Reger J D 1992 *Adv. Phys.* **41** 547
[11] Höchli U T, Knorr K and Loidl A 1990 *Adv. Phys.* **39** 405
[12] Launer S, le Maire M, Schaack G and Haussühl S 1992 *Ferroelectrics* **135** 257
[13] Albers J, Klöpperpieper A, Rother H J and Haussühl S 1988 *Ferroelectrics* **81** 27
[14] Paasch M 1991 *Thesis* University of Mainz
[15] Narz T 1991 *PhD Thesis* University of Köln
[16] Fesh I, Paasch M, Hutton S L, Braune M, Böhmer R, Loidl A, Dörffel M, Narz Th, Haussühl S and McIntyre G J, 1993 *Ferroelectrics* **138** 1
[17] Pöppl A, Völker G, Metz H and Klöpperpieper A 1994 *Phys. Status Solidi* b **184** 471
Bauch H, Böttcher R and Völker G 1993 *Phys. Status Solidi* b **178** k39
[18] Santos M L, Chaves M R, Almeida A, Klöpperpieper A, Müser H E and Albers J 1993 *Ferroelectr. Lett.* **15** 17
[19] Banys J, Klimm C, Völker G, Bauch H and Klöpperpieper A 1994 *Phys. Rev.* B **50** 16751
[20] Sobestrianskas R, Grigas J, Czapla Z and Dacko S 1993 *Phys. Status Solidi* a **136** 223
[21] Courtens E 1984 *Phys. Rev. Lett.* **52** 69
[22] le Maire M and Schaack G 1995 *Proc. 3rd Int. Symp. on Domain Structure of Ferroelectrics and Related Materials (Zakopane, Poland, 1994); Ferroelectrics* at press
[23] Koch G and Happ H 1993 *Ann. Phys., Lpz.* **2** 522
[24] Freitag O, Brückner H J and Unruh H G 1985 *Z. Phys.* B **61** 75
[25] Schrader B 1989 *Raman/IR Atlas of Organic Compounds* (Weinheim: VCH-Verlagsgesellschaft)
[26] Tsuboi M 1957 *J. Am. Chem. Soc.* **79** 1351
[27] Herzberg G 1945 *Infrared and Raman Spectra* (New York: Van Nostrand Reinhold)
[28] Goncharov Yu G, Kozlov G V, Volkov A A, Albers J and Petzelt J 1988 *Ferroelectrics* **80** 221